

Estimation of Reciprocal Residual Flexibility from Experimental Modal Data

Scott W. Doebling*

Los Alamos National Laboratory, Los Alamos, NM, 87545

Lee D. Peterson†

University of Colorado, Boulder, CO, 80309-0429

Kenneth F. Alvin‡

Sandia National Laboratories, Albuquerque, NM, 87185-0439

Abstract

A technique is presented for estimating the residual flexibility between non-excited structural degrees of freedom from experimental structural vibration data. Using this method, the residual flexibility estimated from modal measurements can be included in the computation of measured flexibility for experiments with incomplete reciprocity, i.e. when the response and excitation measurement sensors are not fully collocated. The method can also be used to estimate the unknown entries in the residual flexibility matrix for experimental component mode synthesis when excitations are not provided at all interface degrees of freedom. A general solution is presented which contains an unknown positive semidefinite contribution. The general solution satisfies modal orthogonality in the limit that all of the structural degrees of freedom are instrumented and when the positive semidefinite contribution lies in a nullspace defined by the stiffness matrix and the modal flexibility. With a

*Postdoctoral Research Associate, Engineering Sciences and Applications Division, Engineering Analysis Group (ESA-EA), Mail Stop P946, Los Alamos National Laboratory, Los Alamos, NM, 87545. Member AIAA.

†Associate Professor, Center for Aerospace Structures and Department of Aerospace Engineering Sciences, University of Colorado, Boulder, CO, 80309-0429. Senior Member AIAA.

‡Senior Member of Technical Staff, Structural Dynamics and Vibration Control Department, Sandia National Laboratories, Albuquerque, NM, 87185-0439. Member AIAA.

limited number of measurements, modal orthogonality is shown to be satisfied to the extent that the measured modes are preserved by static condensation. A rank-deficient solution is presented which allows the residual to be used in the computation of the flexibility matrix without further modeling assumptions. Numerical and experimental results are presented which demonstrate the application of the method to both flexibility matrix convergence and to experimental component mode synthesis.

Nomenclature

$[G]$	Flexibility matrix
$[G_r]$	Residual flexibility matrix
$[H(\omega)]$	Frequency response function matrix
$[\bar{K}]$	Statically condensed stiffness matrix
$[M_r]$	Residual mass
$[M], [K]$	Mass and stiffness matrices
$\{q\}$	Generalized coordinate basis
$[T]$	Arbitrary orthonormal transformation
$\{x\}$	Generalized displacement vector
$[\Phi]$	Mode shape matrix
$[\Lambda]$	Modal eigenvalue matrix ($\text{diag}\{\omega^2\}$)
ω	Circular modal frequency

Subscripts (Instrumentation Degrees of Freedom)

d	Instrumented degrees of freedom which are driving points
-----	--

(excitation and response)

m	Instrumented (“measured”) degrees of freedom
o	Non-instrumented (“omitted”) degrees of freedom
s	Instrumented degrees of freedom which are not driving points (response only)

Subscripts (Modal Degrees of Freedom)

n	Measured modal set
r	Residual modal set

Superscripts (Solution Methods)

o	Rank-deficient solution
-----	-------------------------

Introduction

Modeling the dynamic behavior of structures is accomplished using both analytical and experimental techniques. In many methods, the measured data from a vibration experiment is used to refine or modify a finite element model (FEM) so that the model more closely predicts the observed dynamics of the structure.^{1,2,3} These techniques have also been applied to the problem of structural damage detection by using the measured modes of the damaged structure in the update so that the resulting model reflects the changes in the structural properties. However, the use of individual measured modes in the update produces some difficulties, such as the selection of which measured modes to use.⁴ For this reason, and because of other difficulties inherent in dynamic FEM update, the flexibility matrix is gaining use as a tool for modeling structures based on experimental data.

The structural flexibility matrix can be estimated using only the measured mode shapes and measured modal frequencies. In the limit that all structural modes are measured, the

measured flexibility matrix asymptotically approaches the inverse of the structural stiffness matrix; i.e. the flexibility matrix is the static structural response to an applied static load vector. It is this property of the flexibility matrix which makes it a useful and intuitive tool for damage detection and model update. Recently, the measured flexibility matrix has been used for damage detection in bridges^{5,6,7} and aircraft skin.^{6,8}

Previous approaches to the measurement of the flexibility matrix have focused only on the contributions of the identified vibration modes, the so-called “modal flexibility.” However, the structural modes not in the identified modal set, the “residual modes,” also contribute to the flexibility of the structure. This contribution is called “residual flexibility,” and it can be estimated in conjunction with the measured modes from the measured frequency response functions (FRF). The difficulty involved in using the residual flexibility is that it can only be computed between the test excitation degrees of freedom (DOF) and the test response DOF, so it has dimension $(m \times d)$. The modal flexibility, on the other hand, is defined between each pair of response DOF (i.e. it is “fully reciprocal”) so that it has dimension $(m \times m)$. Thus, the residual and modal flexibility matrices cannot be added together since their dimensions are incompatible.

However, if the unmeasured partition of the residual flexibility matrix can be estimated, the accuracy of the measured flexibility matrix can be improved. Generally, the contribution of the residual flexibility is only about 3% - 10% of the modal flexibility, but for applications such as model refinement and damage detection, this level of improved accuracy can be very important. For example, Toksoy and Aktan⁵ state that the modal flexibility for their particular experiment is about 90% of the total flexibility. Inclusion of the estimated residual contribution for this experiment could make such results even more accurate.

An important application of measured flexibility which requires measurement of the residual flexibility is experimental component mode synthesis (CMS). This is a modeling technique which combines substructure models together in the form of the measured modes and the measured residual flexibility matrix. Key references in the development of experimental CMS are MacNeal⁹, Rubin¹⁰, Craig and Chang¹¹, and Martinez, et al.¹² This method has been applied to test structures to model fixed-base dynamic behavior using free-free modal test results.^{13,14} In the basic implementation, an excitation input is required at each interface DOF (the locations where the substructures are to be joined together). The method developed in this paper alleviates this strict input placement technique, so that excitation inputs would only be required at a subset of the interface DOF.

In this paper, a method is presented for estimating the fully reciprocal residual flexibility matrix using only the measured partition of the residual flexibility. A rank-deficient particular solution is proposed which uses only the measured data and requires no further modeling assumptions or FEM. This rank-deficient solution is applied to continuous analytical beam models and to experimental data from a cantilevered beam structure to demonstrate improvements in accuracy for both dynamically measured flexibility and experimental CMS.

The remainder of this paper is organized as follows: First, the general inverse vibration problem is presented, which includes a derivation of the relationship between the structural stiffness matrix, the structural flexibility matrix, and the measured modes. This section also defines the measured degrees of freedom, and partitions the full flexibility matrix accordingly. Second, the technique for estimating the non-reciprocal residual flexibility matrix partition from the measured FRF data is presented. Next, the general solution for the un-

measured partition of the flexibility matrix is presented. The satisfaction of the modal orthogonality condition by this solution is demonstrated next, and then the rank-deficient solution is derived. Finally, the numerical and experimental applications are presented.

Computing Flexibility Using Inverse Vibration

Suppose that the undamped free vibration of a structural dynamic system is described by the $(N \times N)$ second-order differential equation

$$[M]\{\ddot{x}\} + [K]\{x\} = 0 \quad (1)$$

The eigensolution of this system consists of the eigenvalue matrix $[\Lambda]$, which is a diagonal matrix of the squared natural frequencies, $\text{diag}\{\omega_k^2\}$, and the eigenvector matrix $[\Phi]$, which is mass-normalized such that

$$\begin{aligned} [\Phi]^T[K][\Phi] &= [\Lambda] \\ [\Phi]^T[M][\Phi] &= [I] \end{aligned} \quad (2)$$

Solving the first equation in Eq. (2) for the stiffness matrix yields

$$[K] = [\Phi]^{-T}[\Lambda][\Phi]^{-1} = ([\Phi][\Lambda]^{-1}[\Phi]^T)^{-1} \quad (3)$$

The flexibility is defined as the inverse of the stiffness matrix. However, when the structure has one or more rigid body modes, $[K]$ is rank deficient. In this case, $[G]$ is defined as the “Moore-Penrose pseudoinverse”¹⁵ of $[K]$

$$[G] \equiv [K]^+ = [\Phi][\Lambda]^{-1}[\Phi]^T \quad (4)$$

and $[\Lambda]$ is defined to contain only the flexible modes of the system.

Next, the flexibility matrix is separated into a modal component and a residual component, to represent the case when only a subset of the structural vibration modes are measured. Defining the measured modal set as $\{q_n\}$ and the unmeasured (residual) set as

$\{q_r\}$, the eigensolution can be partitioned as

$$\begin{aligned}\Phi &= \begin{bmatrix} \Phi_n & \Phi_r \end{bmatrix} \\ \Lambda &= \begin{bmatrix} \Lambda_n & 0 \\ 0 & \Lambda_r \end{bmatrix}\end{aligned}\tag{5}$$

Substituting Eq. (5) into Eq. (4) yields

$$\begin{aligned}[G] &= [\Phi][\Lambda]^{-1}[\Phi]^T \\ &= \begin{bmatrix} \Phi_n & \Phi_r \end{bmatrix} \begin{bmatrix} \Lambda_n & 0 \\ 0 & \Lambda_r \end{bmatrix}^{-1} \begin{bmatrix} \Phi_n & \Phi_r \end{bmatrix}^T \\ &= [\Phi_n][\Lambda_n]^{-1}[\Phi_n]^T + [\Phi_r][\Lambda_r]^{-1}[\Phi_r]^T \\ &= [G_n] + [G_r]\end{aligned}\tag{6}$$

where $[G_n]$ is the modal flexibility, formed from the measured modes and frequencies as

$$[G_n] = [\Phi_n][\Lambda_n]^{-1}[\Phi_n]^T\tag{7}$$

and $[G_r]$ is the residual flexibility, formed from the residual modes and frequencies as

$$[G_r] = [\Phi_r][\Lambda_r]^{-1}[\Phi_r]^T\tag{8}$$

In practice, the measured flexibility matrix is not computed for the full DOF set, because only a limited number of measurements are available. Partitioning the full DOF set $\{q\}$ into the instrumented DOF, $\{q_m\}$, and the non-instrumented (omitted) DOF, $\{q_o\}$ yields

$$\{q\} = \begin{Bmatrix} q_m \\ q_o \end{Bmatrix}\tag{9}$$

Further partitioning the modal vectors of Eq. (5) yields the modally and spatially partitioned mode shape matrix

$$\Phi = \begin{bmatrix} \Phi_n & \Phi_r \end{bmatrix} = \begin{bmatrix} \Phi_m \\ \Phi_o \end{bmatrix} = \begin{bmatrix} \Phi_{n_m} & \Phi_{r_m} \\ \Phi_{n_o} & \Phi_{r_o} \end{bmatrix} \quad (10)$$

In this notation, the columns of $[\Phi_{n_m}]$ are the measured mode shapes sampled at the sensor DOF for the measured modes. These are usually referred to simply as the “measured mode shapes.” Substituting Eq. (10) into Eq. (4) yields an expression for the fully partitioned flexibility matrix

$$\begin{aligned} [G] &= [\Phi][\Lambda]^{-1}[\Phi]^T \\ &= \begin{bmatrix} \Phi_{n_m} & \Phi_{r_m} \\ \Phi_{n_o} & \Phi_{r_o} \end{bmatrix} \begin{bmatrix} \Lambda_n & 0 \\ 0 & \Lambda_r \end{bmatrix}^{-1} \begin{bmatrix} \Phi_{n_m} & \Phi_{r_m} \\ \Phi_{n_o} & \Phi_{r_o} \end{bmatrix}^T \\ &= \begin{bmatrix} G_{mm} & G_{mo} \\ G_{mo}^T & G_{oo} \end{bmatrix} \end{aligned} \quad (11)$$

As shown by Alvin, et al.^{16,17} the inverse of the measured flexibility is equal to the Guyan-reduced (or statically condensed) system stiffness matrix¹⁸ with respect to the measured DOF set $\{q_m\}$

$$[G_{mm}]^{-1} = [K_{mm}] - [K_{mo}][K_{oo}]^{-1}[K_{mo}]^T \quad (12)$$

where the partitions of $[K]$ are defined as

$$[K] = \begin{bmatrix} K_{mm} & K_{mo} \\ K_{mo}^T & K_{oo} \end{bmatrix} \quad (13)$$

In order to be explicit about the form of the measured flexibility, it is necessary to further partition the measured flexibility with respect to the driving point DOF, $\{q_d\}$, and the response sensor DOF (with no excitation inputs), $\{q_s\}$. So the measured DOF are partitioned as

$$\{q_m\} = \begin{Bmatrix} q_d \\ q_s \end{Bmatrix} \quad (14)$$

For this research, it will be assumed that each excitation input DOF contains a collocated response sensor, so that $\{q_d\}$ describes the full set of driving point DOF. The measured DOF partition of the mode shape matrix is further partitioned as

$$[\Phi_m] = \begin{bmatrix} \Phi_{n_m} & \Phi_{r_m} \end{bmatrix} = \begin{bmatrix} \Phi_{n_d} & \Phi_{r_d} \\ \Phi_{n_s} & \Phi_{r_s} \end{bmatrix} \quad (15)$$

and the measured flexibility matrix is partitioned as

$$[G_{mm}] = \begin{bmatrix} G_{dd} & G_{sd}^T \\ G_{sd} & G_{ss} \end{bmatrix} \quad (16)$$

$[G_{mm}]$ is a statically complete representation of the structural response between the instrumented DOF $\{q_m\}$. Combining Eq. (16) with Eq. (6), the modal and residual contributions to the measured flexibility matrix can be partitioned as

$$\begin{bmatrix} G_{dd} & G_{sd}^T \\ G_{sd} & G_{ss} \end{bmatrix} = \begin{bmatrix} G_{n_{dd}} & G_{n_{sd}}^T \\ G_{n_{sd}} & G_{n_{ss}} \end{bmatrix} + \begin{bmatrix} G_{r_{dd}} & G_{r_{sd}}^T \\ G_{r_{sd}} & G_{r_{ss}} \end{bmatrix} \quad (17)$$

As shown in the next section, all of the partitions on the right side of Eq. (17) can be identified directly from the measured data, except for $[G_{r_{ss}}]$.

Estimation of Residual Flexibility from Modal Data

This section demonstrates how the measured FRF matrix $[H(\omega)]$ can be partitioned to show the effects of residual flexibility. If the measurement sensors are accelerometers, then the inertance (force to acceleration) FRF for response at DOF i due to excitation at DOF j

can be written as a sum over all the structural modes

$$H_{ij}(\omega) = -\omega^2 \left(\sum_{k=1}^{\infty} \frac{\phi_k^i \phi_k^j}{\omega_k^2 - \omega^2} \right) \quad (18)$$

where $\{\phi_k\}$ is the k^{th} mode shape and ω_k is the k^{th} modal frequency. A complete discussion of the estimation and form of the frequency response function can be found in Ewins.¹⁹

The source of residual flexibility can be seen by separating the FRF into the components below and above the bandwidth of measurement. Suppose that there are n_1 modes below the measured bandwidth (including rigid-body modes) and n_2 modes in the measured bandwidth. The FRF of Eq. (18) can then be written as

$$H_{ij}(\omega) = -\omega^2 \left(\sum_{k=1}^{n_1} \frac{\phi_k^i \phi_k^j}{\omega_k^2 - \omega^2} + \sum_{k=n_1+1}^{n_1+n_2} \frac{\phi_k^i \phi_k^j}{\omega_k^2 - \omega^2} + \sum_{k=n_1+n_2+1}^{\infty} \frac{\phi_k^i \phi_k^j}{\omega_k^2 - \omega^2} \right) \quad (19)$$

For the first term of Eq. (19), representing the modes below the bandwidth, the limit as $\omega \gg \omega_k$ is

$$\lim_{\frac{\omega_k}{\omega} \rightarrow 0} \left\{ -\omega^2 \sum_{k=1}^{n_1} \frac{\phi_k^i \phi_k^j}{\omega_k^2 - \omega^2} \right\} = \sum_{k=1}^{n_1} \phi_k^i \phi_k^j \quad (20)$$

Since this is a constant term relating force to acceleration, the effect of these low-frequency modes is analogous to a mass (or inertia) term. It is called “residual mass” by MacNeal⁹ and “residual inertance” by Admire, et al.¹³ (As noted in Reference [13], this term does not exist in Rubin’s nomenclature¹⁰ since Rubin retains the rigid body modes in the normal mode set and assumes that there are no unmeasured flexible modes below the test bandwidth.)

For the third term of Eq. (19), writing a MacLaurin series expansion and taking the limit

as $\omega \ll \omega_k$ yields

$$\lim_{\frac{\omega}{\omega_k} \rightarrow 0} \left\{ -\omega^2 \sum_{k=n_1+n_2+1}^{\infty} \frac{\phi_k^i \phi_k^j}{\omega_k^2 - \omega^2} \right\} = \quad (21)$$

$$-\omega^2 \left\{ \sum_{k=n_1+n_2+1}^{\infty} \frac{\phi_k^i \phi_k^j}{\omega_k^2} \right\} + \omega^4 \left\{ \sum_{k=n_1+n_2+1}^{\infty} \frac{\phi_k^i \phi_k^j}{\omega_k^4} \right\} - \dots$$

The first term on the right side of Eq. (21) (proportional to ω^2) approximates an inverse stiffness term, thus it is referred to as “residual flexibility.” The second term (proportional to ω^4) is used in Rubin’s formulation of the component mode model; Rubin¹⁰ refers to this term as “residual inertia,” and Admire, et al.¹³ refer to it as “residual mass.” This term does not exist in the formulation of MacNeal.⁹

As demonstrated by Peterson and Alvin²⁰ and Doebling, et al.²¹, the time domain state-space model is often insufficient to accurately reproduce the frequency domain characteristics of the modal vibration data, particularly near areas of low structural response. One reason for this is the inability of the time-domain equations to represent the contribution of the residual flexibility. Therefore, a technique has been developed to use the pole information from a variant on the Eigensystem Realization Algorithm²² to estimate the mode shapes concurrently with the residual flexibility and residual mass terms in the frequency domain.²⁰ Consequently, the mode shapes and residuals are both obtained such that the identified model more accurately reproduces the measured data. This technique has been demonstrated to be more accurate than the traditional method, which uses “residual functions.”¹⁹

Only part of the residual flexibility matrix with respect to the instrumented DOF is measurable from the data. Rewriting Eq. (19) yields

$$H(\omega) = -\omega^2[\Phi_{n_m}][(\Lambda_n) - \omega^2[I]]^{-1}[\Phi_{n_d}] - \omega^2[G_{r_d}] + [M_{r_d}] \quad (22)$$

where $[G_{r_d}]$ is the measured partition of residual flexibility, such that

$$[G_{r_d}] = [\Phi_{r_m}][\Lambda_r]^{-1}[\Phi_{r_d}]^T \quad (23)$$

To see the correspondence between the full residual flexibility matrix $[G_r]$ and the measured residual flexibility $[G_{r_d}]$, obtain the modal parameterization of the residual flexibility matrix by substituting the expression for $[\Phi_{r_m}]$ in Eq. (15) into the expression for $[G_r]$ in Eq. (8). This yields the modal expansion for the full residual flexibility matrix

$$[G_r] = \begin{bmatrix} \Phi_{r_d}\Lambda_r^{-1}\Phi_{r_d}^T & \Phi_{r_d}\Lambda_r^{-1}\Phi_{r_s}^T \\ \Phi_{r_s}\Lambda_r^{-1}\Phi_{r_d}^T & \Phi_{r_s}\Lambda_r^{-1}\Phi_{r_s}^T \end{bmatrix} = \begin{bmatrix} G_{r_{dd}} & G_{r_{sd}}^T \\ G_{r_{sd}} & G_{r_{ss}} \end{bmatrix} \quad (24)$$

Expanding Eq. (23), the residual flexibility matrix estimated from the measured FRF matrix can be written in terms of modal partitions as

$$[G_{r_d}] = [\Phi_{r_m}][\Lambda_r]^{-1}[\Phi_{r_d}]^T = \begin{bmatrix} \Phi_{r_d} \\ \Phi_{r_s} \end{bmatrix} [\Lambda_r]^{-1} [\Phi_{r_d}]^T = \begin{bmatrix} \Phi_{r_d}\Lambda_r^{-1}\Phi_{r_d}^T \\ \Phi_{r_s}\Lambda_r^{-1}\Phi_{r_d}^T \end{bmatrix} \quad (25)$$

It is apparent by comparison of Eq. (24) and Eq. (25) that the measured and parameterized partitions correspond as

$$[G_{r_d}] = \begin{bmatrix} G_{r_{dd}} \\ G_{r_{sd}} \end{bmatrix} \quad (26)$$

Thus, the columns of $[G_{r_d}]$ are the columns of $[G_r]$ which correspond to the driving point DOF, so the estimated residual flexibility matrix $[G_{r_d}]$ has dimensions $(m \times d)$.

Because of the relationship shown in Eq. (26), a driving point response must be obtained at every DOF at which a column of the residual flexibility matrix is desired. To ob-

tain a fully reciprocal flexibility matrix, this means exciting the structure at every DOF in $\{q_m\}$, such that $\{q_d\} = \{q_m\}$. This constraint generally adds time and cost to the measurement of the flexibility matrix, due to the sometimes large number of excitations required. Since the selection of the excitation DOF $\{q_d\}$ determines which columns of $[G_r]$ are known, it will determine, in part, the accuracy of the estimated residual. This excitation location consideration is discussed in Reference [6].

To relax this strict input placement requirement, it is necessary to somehow compute the unmeasured partition of the residual flexibility matrix. This is necessary so that the residual flexibility will be known with respect to the entire measurement DOF set and not just the driving point DOF. Due to reciprocity, the upper right partition of $[G_r]$ is known to be the transpose of the lower left partition, as shown in Eq. (24). Thus only one partition of the residual flexibility matrix is unknown: $[G_{r_{ss}}]$.

General Solution for Unmeasured Partition of Residual Flexibility

A general solution for the unmeasured partition of the residual flexibility matrix $[G_{r_{ss}}]$ can be written by parameterizing the residual flexibility matrix in terms of the residual mode shapes and modal frequencies. As shown in Eq. (24), this partition can be written as

$$[G_{r_{ss}}] = [\Phi_r][\Lambda_r]^{-1}[\Phi_r]^T \quad (27)$$

Using the expression for $[G_{r_{dd}}]$ from Eq. (24), we can state without loss of generality that

$$[\Phi_r][\Lambda_r]^{-1/2} = \begin{bmatrix} [G_{r_{dd}}]^{1/2} & 0 \end{bmatrix} [T] \quad (28)$$

where $[T]$ is some unknown orthonormal transformation such that

$$[T][T]^T = [T]^T[T] = [I] \quad (29)$$

and $[G_{r_{dd}}]^{1/2}$ is a symbolic Cholesky factorization²³ of $[G_{r_{dd}}]$. Since the number of residual modes is generally much larger than the number of driving point DOF, the residual mode shapes and modal frequencies cannot be determined exactly. The orthonormal matrix $[T]$ in Eq. (28) represents a transformation to an unknown coordinate basis, so that the decomposition is general. Then, using Eq. (28) together with the expression for $[G_{r_{sd}}]$ from Eq. (24), we have

$$[\Phi_{r_s}][\Lambda_r]^{-1/2} = \left[[G_{r_{sd}}]([G_{r_{dd}}]^{1/2})^{-T} [X] \right] [T] \quad (30)$$

where $[X]$ is an arbitrary matrix of dimension $(s \times r)$.

The decompositions of Eq. (28) and Eq. (30) are the most general forms necessary to describe the possible parameterizations of the corresponding partitions of $[G_r]$ as shown in Eq. (24). Since $[T]$ is arbitrary, each of these decompositions are general in the sense that they may be expressed in any coordinate basis. To see that Eq. (28) satisfies Eq. (24), multiply each side by its own transpose to get

$$\begin{aligned} & ([\Phi_{r_d}][\Lambda_r]^{-1/2})([\Phi_{r_d}][\Lambda_r]^{-1/2})^T = \\ & \left(\begin{bmatrix} [G_{r_{dd}}]^{1/2} & 0 \end{bmatrix} [T] \right) \left(\begin{bmatrix} [G_{r_{dd}}]^{1/2} & 0 \end{bmatrix} [T] \right)^T \end{aligned} \quad (31)$$

This reduces to

$$[\Phi_{r_d}][\Lambda_r]^{-1}[\Phi_{r_d}]^T = [G_{r_{dd}}] \quad (32)$$

which corresponds to the upper left partition of Eq. (24). To see that Eq. (30) satisfies Eq. (24), multiply Eq. (30) by the transpose of Eq. (28) to get

$$([\Phi_{r_s}][\Lambda_r]^{-1/2})([\Phi_{r_d}][\Lambda_r]^{-1/2})^T = \left(\begin{bmatrix} [G_{r_{sd}}]([G_{r_{dd}}]^{1/2})^{-T} [X] [T] \end{bmatrix} \begin{bmatrix} [G_{r_{dd}}]^{1/2} & 0 \end{bmatrix} [T] \end{bmatrix}^T \right) \quad (33)$$

This reduces to

$$[\Phi_{r_s}][\Lambda_r]^{-1}[\Phi_{r_d}]^T = [G_{r_{sd}}] \quad (34)$$

which corresponds to the lower left partition of Eq. (24). The matrix $[X]$ is arbitrary since it multiplies the zero partition of Eq. (28), as shown in Eq. (33). Thus, Eq. (28) and Eq. (30) are expressed in an arbitrary coordinate basis, and satisfy the constraints of Eq. (24).

Substituting Eq. (30) into Eq. (27) yields the general solution for $[G_{r_{ss}}]$ as

$$[G_{r_{ss}}] = [G_{r_{sd}}][G_{r_{dd}}]^{-1}[G_{r_{sd}}]^T + [X][X]^T \quad (35)$$

This general solution for the unmeasured partition of the residual flexibility matrix effectively parameterizes all possible solutions in terms of the positive semidefinite symmetric matrix $[X][X]^T$. Constraints can be placed on the form of this matrix by applying additional conditions on the general solution.

Satisfaction of Modal Orthogonality by General Solution

This section shows how the matrix $[X]$ of Eq. (35) can be chosen such that the condition of stiffness orthogonality between measured and residual modes is satisfied by the general solution of $[G_{r_{ss}}]$ in the limit that all of the structural DOF are instrumented. Presume $[\Phi]$ is the set of eigenmodes for the $(N \times N)$ system stiffness matrix $[K]$, normalized as in Eq. (2). For $i \neq j$, $\{\Phi_i\}$ and $\{\Phi_j\}$ are stiffness-orthogonal, such that

$$\{\Phi_i\}^T [K] \{\Phi_j\} = 0 \quad (36)$$

If $[\Phi]$ is then partitioned into measured modes $[\Phi_n]$ and residual modes $[\Phi_r]$, by Eq. (36)

these modes must be stiffness-orthogonal. This condition can be written

$$[\Phi_n]^T [K] [\Phi_r] = 0 \quad (37)$$

Pre-multiplying Eq. (37) by $[\Phi_n][\Lambda_n]^{-1}$ and post-multiplying by $[\Lambda_r]^{-1}[\Phi_r]^T$ yields the condition

$$[G_n][K][G_r] = 0 \quad (38)$$

where $[G_n]$ and $[G_r]$ are the full $(N \times N)$ modal and residual flexibility matrices. Thus, Eq. (38) defines the stiffness orthogonality condition between the modal and residual flexibility matrices.

Partitioning $[K]$ into columns corresponding to the driving point DOF, $\{q_d\}$, and non-driving point DOF, $\{q_s\}$, yields

$$[K] = \begin{bmatrix} K_d & K_s \end{bmatrix} \quad (39)$$

where, for the purposes of this derivation, all DOF are assumed to be instrumented, i.e., $\{q_m\}$ contains all N DOF, and $\{q_o\}$ is null. Substituting Eq. (24) and Eq. (39) into Eq. (38) yields

$$[G_n] \begin{bmatrix} K_d & K_s \end{bmatrix} \begin{bmatrix} G_{r_{dd}} & G_{r_{sd}}^T \\ G_{r_{sd}} & G_{r_{ss}} \end{bmatrix} = 0 \quad (40)$$

The equations in the left and right partitions can be expanded to get

$$[G_n][K_d][G_{r_{dd}}] + [G_n][K_s][G_{r_{sd}}] = 0 \quad (41)$$

$$[G_n][K_d][G_{r_{sd}}]^T + [G_n][K_s][G_{r_{ss}}] = 0 \quad (42)$$

Assuming $[G_{r_{dd}}]$ is invertible, which is true when the number of residual modes is greater than the number of driving point DOF, Eq. (41) can be solved for $[G_n][K_d]$ to get

$$[G_n][K_d] = -[G_n][K_s][G_{r_{sd}}][G_{r_{dd}}]^{-1} \quad (43)$$

Substituting Eq. (43) into Eq. (42) yields

$$[G_n][K_s][G_{r_{ss}}] = [G_n][K_s][G_{r_{sd}}][G_{r_{dd}}]^{-1}[G_{r_{sd}}]^T \quad (44)$$

Substituting the general solution for $[G_{r_{ss}}]$ from Eq. (35) into Eq. (44) and reducing yields

$$[G_n][K_s][X][X]^T = 0 \quad (45)$$

Thus, the contribution $[X][X]^T$ to the general solution Eq. (35) must lie in the right null space of $[G_n][K_s]$. Unfortunately, since $[K_s]$ is itself unknown, this condition cannot be used to directly construct $[X][X]^T$. Also, this condition is strictly true only when the full structural DOF set is measured.

As described in Reference [6], the limited set of modal response measurements do not allow computation of the full stiffness matrix $[K]$, but only the Guyan-reduced stiffness with respect to the measured DOF, $\overline{[K]}$. Since it is desirable to express the orthogonality condition purely in terms of measurable quantities, the orthogonality relation of Eq. (45) can be reduced to the measurement DOF, $\{q_m\}$ to obtain⁶

$$[G_n][\overline{[K_s]}][X][X]^T = 0 \quad (46)$$

where $\overline{[K_s]}$ are the columns of the statically reduced stiffness matrix corresponding to the non-excited DOF $\{q_s\}$. This reduced form of the orthogonality constraint is important, because it corresponds to the measured partitions of the modal and residual flexibility. Thus Eq. (46) is the form of the orthogonality constraint which is applicable to the experimentally measured quantities. Because of the assumption of static condensation, however, Eq. (46) is only satisfied to the extent that the modes are well-preserved by the static condensation. This condition can sometimes be satisfied when the measured modes have low fre-

quency, and when all DOF of significant mass excited by that mode are instrumented.

Rank-Deficient Solution for Unmeasured Partition

It is possible to derive a solution for the unmeasured partition of the residual flexibility $[G_{r_{ss}}]$ without making further assumptions about the form of the full structural stiffness matrix by simply choosing $[X] = 0$ in Eq. (35). This produces a rank-deficient solution for $[G_{r_{ss}}]$ of the form

$$[G_{r_{ss}}^o] = [G_{r_{sd}}][G_{r_{dd}}]^{-1}[G_{r_{sd}}]^T \quad (47)$$

The advantage of this solution is that it does not require any additional information or assumptions about the structure beyond the measured partitions of the residual flexibility matrix. The disadvantage is that since no information is added, no additional information is available to define the residual modal subspace. Thus the residual flexibility matrix $[G_r]$ has the same rank as $[G_{r_d}]$, which is typically the number of driving points d . Also, since $[X][X]^T$ is always positive semidefinite, Eq. (47) can be considered a lower bound on the true value of $[G_{r_{ss}}]$.

The rank-deficient estimate of $[G_{r_{ss}}]$ computed in $[G_{r_{ss}}^o]$ allows the definition of a rank-deficient solution for the flexibility matrix, $[G^o]$, which can be computed as

$$[G^o] = [\Phi_n][\Lambda_n]^{-1}[\Phi_n]^T + \begin{bmatrix} G_{r_{dd}} & G_{r_{sd}}^T \\ G_{r_{sd}} & G_{r_{ss}}^o \end{bmatrix} \quad (48)$$

where $[\Phi_n]$, $[\Lambda_n]$, $[G_{r_{dd}}]$ and $[G_{r_{sd}}]$ are identified from the measured FRF, and $[G_{r_{ss}}^o]$ is computed using Eq. (47). Thus, an estimate of the measured flexibility matrix which includes the residual flexibility and requires only the measured data is obtained.

In the limit that the driving points span the space of the residual modes, Eq. (47) is the exact solution for $[G_{r_{ss}}]$. This can be proven by substituting the modal parameterizations of $[G_{r_{dd}}]$ and $[G_{r_{sd}}]$ from Eq. (24) into Eq. (47) to get

$$[G_{r_{ss}}^o] = ([\Phi_{r_s}][\Lambda_r]^{-1}[\Phi_{r_d}]^T)([\Phi_{r_d}][\Lambda_r]^{-1}[\Phi_{r_d}]^T)^{-1}([\Phi_{r_d}][\Lambda_r]^{-1}[\Phi_{r_s}]^T) \quad (49)$$

When the number and location of the driving points is sufficient to span the residual modal subspace, $[\Phi_{r_d}]$ is invertible, so Eq. (49) reduces to

$$[G_{r_{ss}}^o] = [\Phi_{r_s}][\Lambda_r]^{-1}[\Phi_{r_s}]^T \quad (50)$$

which is equivalent to the exact modal parameterization of $[G_{r_{ss}}]$ shown in Eq. (27).

Numerical Examples

Example 1: Improved Estimation of Flexibility for 2-DOF Cantilevered Beam

This numerical example demonstrates how the rank-deficient residual flexibility solution described by Eq. (47) and Eq. (48) can be used to estimate the unmeasured partition of the residual flexibility matrix. The application of this flexibility estimation technique is demonstrated for the cantilevered beam model and properties shown in Figure 1. The modes for this example were generated using the continuous solution to the fourth-order boundary value problem for a Bernoulli-Euler beam.²⁴ The modes were mass-normalized numerically.

Consider the 2-DOF model with an input at the vertical tip DOF, so that the DOF sets are defined as

$$\{q_m\} = \begin{Bmatrix} w_1 \\ \theta_1 \end{Bmatrix} \quad \{q_d\} = \{w_1\} \quad \{q_s\} = \{\theta_1\} \quad (51)$$

The stiffness matrix for this structure is²⁵

$$[K] = \begin{bmatrix} 2158.2 & 1618.7 \\ 1618.7 & 1618.7 \end{bmatrix} \left(\frac{N}{m} \right) \quad (52)$$

so that the exact flexibility matrix is

$$[G] = \begin{bmatrix} 1.85 & -1.85 \\ -1.85 & 2.47 \end{bmatrix} \times 10^{-3} \left(\frac{m}{N} \right) \quad (53)$$

For this example, the full residual flexibility matrix is computed by subtracting the measured flexibility of 1 bending mode from the full flexibility matrix. This procedure yields

$$[G_r] = \begin{bmatrix} 5.45 & -20.2 \\ -20.2 & 95.6 \end{bmatrix} \times 10^{-5} \left(\frac{m}{N} \right) \quad (54)$$

Since the excitation is at the first DOF, the measured partition of the residual flexibility $[G_{r_d}]$ is the first column of $[G_r]$, i.e.

$$[G_{r_d}] = \begin{bmatrix} 5.45 \\ -20.2 \end{bmatrix} \times 10^{-5} \quad (55)$$

Partitioning the matrix in Eq. (55) further yields the basic partitions of the residual flexibility:

$$\begin{aligned} [G_{r_{dd}}] &= 5.45 \times 10^{-5} \\ [G_{r_{sd}}] &= -20.2 \times 10^{-5} \end{aligned} \quad (56)$$

Then the rank-deficient solution $[G^o]$, can be found by evaluating Eq. (47) to get

$$[G_{r_{ss}}^o] = [G_{r_{sd}}][G_{r_{dd}}]^{-1}[G_{r_{sd}}]^T = 74.9 \times 10^{-5} \quad (57)$$

and then evaluating Eq. (48) to get

$$[G^o] = \begin{bmatrix} 1.85 & -1.85 \\ -1.85 & 2.27 \end{bmatrix} \times 10^{-3} \quad (58)$$

For this example, the error is expressed in terms of the percent error in the 2-Norm of the flexibility matrices, $\|G_n - G\|/\|G\|$ and $\|G^o - G\|/\|G\|$ respectively. So the norm error in the modal flexibility $[G_n]$ is 25% and the norm error in the rank-deficient residual solution $[G^o]$ is 5%. Thus, even with only one column of the residual flexibility matrix known (from the one test input), the rank-deficient flexibility solution reduces the flexibility shape error by a factor of 5 versus the modal flexibility.

Example 2: Improved Component Mode Synthesis Modeling

This example demonstrates how the rank-deficient residual flexibility solution can be used to improve the combined component mode model of two free-free beams in the case where measured residual flexibility values are not available at all interface DOF. Consider two free-free beams in a plane, as shown in Figure 2, which will be joined using Rubin's free-interface CMS procedure.¹⁰ The interface DOF are defined to be w and θ , and the measured mode set for each substructure consists of two rigid body modes and five flexible modes. Suppose that the substructures are only excited at DOF w , so that only one column of the (2×2) residual flexibility matrix is known. The following methods for computing the unmeasured components of the residual flexibility matrix for the implementation of Rubin's method will be compared:

1. Use diagonals of measured partition $[G_{r_d}]$ known (in this case (1×1)), augmented with zeros to estimate $[G_r]$. This method will be called Rubin Option 1.
2. Full measured partition $[G_{r_d}]$ known (in this case (2×1) , plus 1 reciprocal off-diagonal term), augmented with zeros to estimate $[G_r]$. This method will be referred to as Rubin Option 2.

3. Full measured partition $[G_{r_d}]$ known, rank deficient solution used to compute the rank-deficient residual flexibility matrix $[G_r^o]$. This method will be referred to as the Rank-Deficient Solution method.

It should be noted that the residual flexibility matrices computed using these techniques are all generally rank-deficient, so that the practical implementation requires using the higher frequency measured modes to complete the rank. This requirement is a consequence of the basic formulation of Rubin's method.

The modal frequencies obtained using each of the residual flexibility estimation methods are listed in Table 1, and are compared to the "exact" frequencies from a continuous-

Table 1. Comparison of Frequencies from Rubin Model using Various Estimates of Residual Flexibility

Exact (Hz)	Full Residual (Hz)	Rubin Option 1 (Hz)	Rubin Option 2 (Hz)	Rank-Deficient Solution (Hz)
7.36	7.37	8.07	8.07	7.42
20.31	20.32	20.32	20.32	20.32
39.82	39.85	43.22	43.21	40.07
65.82	65.98	65.99	65.99	65.99
98.33	98.83	108.7	108.4	99.44
137.3	138.6	138.7	138.7	138.7
182.8	185.7	209.1	206.8	187.2

beam solution and to the frequencies obtained using Rubin's method with fully known residuals. It is clear from inspection of Table 1 that the Rank-Deficient Solution, which uses the method derived in this paper, provides results which are superior to the other two methods. Therefore it can be stated that the rank-deficient residual flexibility solution can improve the CMS results using Rubin's method when the residuals are not known at each interface DOF. (It is also interesting to note that for Rubin Options 1 and 2, the modes seem

to alternate between being well correlated and being poorly correlated. The modes which are not well correlated are those modes which have relatively large rotations and relatively small displacements at the end points of the beams, and therefore are not well captured in the residual since the residual flexibility is not measured at the rotational DOF.)

Experimental Applications

A series of modal vibration tests was performed on a simple cantilevered beam structure to study the measurement of flexibility when the experiment has incomplete measurement reciprocity. The test setup for this structure is shown in the photo of Figure 3. A schematic of the test structure is shown in Figure 4, including the instrumentation and test input location. To ensure that the global displacements and rotations could be resolved accurately, the offsets of the sensors from the global nodes were carefully measured. The accurate measurement of the offsets is so important that the measurements were made to the exact location of the sensing element within the sensor housing. The applied force level was measured using a piezoelectric force transducer integrated into the tip of the hammer.

The test parameters are summarized in Table 2. The test procedure consisted of impact-

Table 2. Data Acquisition Parameters for Cantilevered Beam Experiment

Parameter Name	Parameter Value
Sample Frequency	500 Hz
Window Length	32.768 sec
Number of Samples	16,384
Test Band of Interest	3 - 180 Hz
Number of Averages	20
Number of Responses	19
Number of Excitations	1
Instrumentation Type	Accelerometers
Excitation Type	Impact Hammer

ing the tip of the beam vertically with the modal hammer and forming the spectra between the excitation force signal and each acceleration response signal. This excitation was applied repeatedly, and the resulting spectra were averaged and normalized by the averaged input power spectrum to form the measured FRF matrix. The modal frequencies, mode shapes, and residual flexibility were extracted from the measured FRF data using the previously described techniques. The identified frequencies, damping ratios, and descriptions of the mode shapes are presented in Table 3.

Table 3. Identified Modes for Cantilevered Beam Experiment

Frequency (Hz)	Damping Ratio (%)	Mode Description
4.34	0.058	First Bending
27.06	0.508	Second Bending
77.55	0.309	Third Bending
149.47	0.378	Fourth Bending

The measured mode shapes and measured residual flexibility were transformed into the coordinates of the translation and rotation of the beam tip, equivalent to the DOF shown in Figure 1. The modal flexibility and the rank-deficient residual flexibility solution were computed using one measured mode, then two measured modes, etc., and the corresponding measured residual flexibility matrices. To see the effects of residual flexibility on the overall magnitude of the flexibility matrix, consider the flexibility convergence plot shown in Figure 5. This plot shows the norm of the modal flexibility matrix, $[G_n]$, and the norm of the rank-deficient residual flexibility solution, $[G^o]$, versus the number of modes kept in the identified modal set. This plot demonstrates the convergence in overall flexibility magnitude obtained by using the rank-deficient solution for the residual flexibility. The improvement is about 6% for 1 measured mode, and decreases steadily with the number of

measured modes, as expected. It should be noted that while the residual flexibility affects the norm of the flexibility matrix significantly for one identified mode, and slightly for two, any identification which captures at least three bending modes will have an insignificant contribution from the residual flexibility.

It is well known in the field of experimental modal analysis that residual flexibility coefficients are difficult to measure accurately due to their small magnitude. The measured residual flexibility values for the cantilevered beam will therefore be compared to the analytically predicted values to estimate the accuracy of the measurements. The residual flexibility matrix at the tip displacement and rotation DOF computed using the rank-deficient residual flexibility solution is

$$[G_r^o] = \begin{bmatrix} 0.0004 & -0.0134 \\ -0.0134 & 0.5561 \end{bmatrix} \times 10^{-3} \quad (59)$$

Using the idealized model of the cantilevered beam structure (as shown in Figure 1), the full static flexibility matrix is given by

$$[G] = \begin{bmatrix} 1.8 & -1.8 \\ -1.8 & 2.4 \end{bmatrix} \times 10^{-3} \quad (60)$$

and the corresponding residual flexibility matrix is

$$[G_r] = \begin{bmatrix} 0.0013 & -0.0149 \\ -0.0149 & 0.2493 \end{bmatrix} \times 10^{-3} \quad (61)$$

Comparing Eq. (61) and Eq. (59), it is seen that the diagonal terms are off by factors of three and two, respectively, but that the off-diagonal terms are only off by about 10%. The discrepancies in the diagonal terms demonstrates the inherent difficulty in estimating the residual flexibility from test data. It is not clear, however, that the model of this structure

adequately captures the true nature of the boundary conditions, so that the comparison to the analytical prediction should not be used as grounds for discounting the experimental results.

The most important thing to note is that the terms estimated using the rank-deficient residual technique will be limited in accuracy by the accuracy of the measured residuals. In fact, in this comparison, the second diagonal term of $[G_r]$, which is the term estimated by the rank-deficient residual flexibility technique, is in fact more accurate than the first diagonal term, which is estimated directly from the measured data. To demonstrate the accuracy of the rank-deficient solution independent of the measurement error, consider the value of $[G_{r_{ss}}^o]$ which would be obtained using the measured partition of the analytical residual flexibility from Eq. (61). This value is 0.1708, as compared to the exact value of 0.2493. So in the case of perfect measurements, the rank-deficient solution would under-predict the correct value by about 30%, but does provide the expected lower bound on the value of $[G_{r_{ss}}]$.

Experience has demonstrated that the level of significance of the residual flexibility varies a great deal depending upon the structure and the boundary conditions. For example, the flexibility convergence plot for a test performed on a planar idealization of an automobile engine cradle is shown in Figure 6. For this data, the difference in the norms of the modal flexibility and rank-deficient flexibility solution values is nearly 100% for 1 mode, and decreases nearly monotonically to almost zero for 12 modes. However, it should be noticed that while the significance of the residual flexibility is much higher than for the cantilevered beam, it still tends to decrease as the number of measured modes increases, since the magnitude of the norm of the modal flexibility also increases.


Conclusion

A method for estimating the fully reciprocal residual flexibility matrix for experimental configurations which have incomplete reciprocity has been presented. A general solution was derived, which was composed of a contribution from the measured partition of the residual flexibility and an unknown positive semidefinite matrix. The general solution was shown to satisfy modal orthogonality when the unknown matrix lied in the nullspace of a partition of the global stiffness matrix, in the limit that all structural DOF were instrumented. The general solution was also shown to satisfy modal orthogonality with a reduced set of instrumented points when the measured modes were approximately preserved by static condensation. A rank-deficient solution was presented which can be computed using only the measured partitions of the residual flexibility matrix, and which is a lower bound on the full-rank residual flexibility matrix.

Numerical and experimental results were presented that demonstrated that while the significance of the contribution of residual flexibility is highly problem dependent, the rank-deficient residual flexibility improved the convergence of the norm of the flexibility matrix for all of the problems considered. These results demonstrate that the use of the rank-deficient flexibility solution should improve the results of any damage detection, model refinement, or CMS algorithm which uses the measured flexibility or residual flexibility matrices.

Acknowledgments

This paper reports work supported by Sandia National Laboratories under Contract No. AJ-4223 with Dr. George H. James III and Dr. John R. Red-Horse as technical monitors.

The authors would like to thank Prof. K.C. Park and Prof.  Los Felippa for their encouragement and valuable technical insights. Also, the authors wish to recognize University of Colorado undergraduate students Ms. Nikki Robinson and Ms. Trudy Schwartz for their invaluable contributions to the experimental portion of this research. The data from the automobile engine cradle was supplied courtesy of Sandia National Laboratories and The General Motors Corporation. Support for the first author was also provided by Los Alamos National Laboratory Directed Research and Development Project #95002. This article is based on a paper presented at the 36th AIAA/ASME/AHS Adaptive Structures Forum in April 1995.

References

¹Hemez, F. M. and Farhat, C. “Structural Damage Detection via a Finite Element Model Updating Methodology,” *International Journal of Analytical and Experimental Modal Analysis*, Vol. 10, No. 3, 1995, pp. 152–166.

²Smith, S. W. and Beattie, C. A., “Model Correlation and Damage Location for Large Space Truss Structures: Secant Method Development and Evaluation”, NASA-CR-188102, Jan. 1991.

³Zimmerman, D. C. and Kaouk, M., “Structural Damage Detection Using a Minimum Rank Update Theory,” *Journal of Vibration and Acoustics*, Vol. 116, April 1994, pp. 222–230.

⁴Doebling, S. W., Hemez, F. M., Barlow, M. S., Peterson, L. D., and Farhat, C., “Selection of Experimental Modal Data Sets for Damage Detection via Model Update,” *Proceedings of the 34th AIAA/ASME/ASCE/AHS/ASC Structures, Structural Dynamics and Materials Conference*, La Jolla, CA, April 1993, pp. 1506–1517.

⁵Toksoy, T. and Aktan, A. E. “Bridge-condition Assessment by Modal Flexibility,” *Experimental Mechanics*, Vol. 34, Sept. 1994, pp. 271–278.

⁶Doebling, S. W., *Measurement of Structural Flexibility Matrices for Experiments with Incomplete Reciprocity*, Ph. D. Dissertation, University of Colorado, Boulder, CO, Department of Aerospace Engineering Sciences, April 1995, Report No. CU-CAS-95-10.

⁷Mayes, R. L. "An Experimental Algorithm for Detecting Damage Applied to the I-40 Bridge over the Rio Grande," *Proceedings of the 13th International Modal Analysis Conference*, Nashville, TN, Feb. 1995, pp. 219–225.

⁸Robinson, N. A., Peterson, L. D., James, G. H., and Doebling, S. W., "Damage Detection in Aircraft Structures Using Dynamically Measured Static Flexibility Matrices," *Proceedings of the 14th International Modal Analysis Conference*, Dearborn, MI, Feb. 1996, pp. 857–865.

⁹MacNeal, R. H., "A Hybrid Method of Component Mode Synthesis," *Computers and Structures*, Vol. 1, 1971, pp. 581–601.

¹⁰Rubin, S., "Improved Component-Mode Representation for Structural Dynamic Analysis," *AIAA Journal*, Vol. 13, No. 8, 1975, pp. 995–1006.

¹¹Craig, R. R., Jr. and Chang, C.-J., "On the Use of Attachment Modes in Substructure Coupling for Dynamic Analysis," *Proceedings of the 18th AIAA/ASME Structures, Structural Dynamics, and Materials Conference*, San Diego, CA, March 1977, pp. 89–99.

¹²Martinez, D. R., Carne, T. G., Gregory, D. L., and Miller, A. K., "Combined Experimental/Analytical Modeling using Component Mode Synthesis," AIAA Paper No. 84–0941, May 1984.

¹³Admire, J. R., Tinker, M. L., and Ivey, E. W., "Residual Flexibility Test Method for Verification of Constrained Structural Models," *AIAA Journal*, Vol. 32, No. 1, 1994, pp. 170–175.

¹⁴Smith, K. S. and Peng, C.-Y., "SIR-C Modal Survey: A Case Study in Free-Free Testing," *Proceedings of the 12th International Modal Analysis Conference*, Honolulu, HI, Jan. 1994, pp. 176–183.

¹⁵Strang, G., *Linear Algebra and its Applications*, Harcourt Brace Jovanovich, San

Diego, 1988.

¹⁶Alvin, K. F., *Second Order Structural Identification via State Space-Based System Realizations*, Ph. D. Dissertation, University of Colorado, Boulder, CO, 1993.

¹⁷Alvin, K. F., Peterson, L. D., and Park, K. C., "Method for Determining Minimum-Order Mass and Stiffness Matrices from Modal Test Data," *AIAA Journal*, Vol. 33, No. 1, 1994, pp. 128-135.

¹⁸Guyan, R. J., "Reduction of Stiffness and Mass Matrices," *AIAA Journal*, Vol. 3, No. 2, 1965, p. 380.

¹⁹Ewins, D. J., *Modal Testing: Theory and Practice*, John Wiley and Sons, New York, 1984.

²⁰Peterson, L. D. and Alvin, K. F., "A Time and Frequency Domain Procedure for Identification of Structural Dynamic Models," AIAA Paper 94-1731, April 1994. Submitted to *Journal of Sound and Vibration*.

²¹Doebling, S. W., Alvin, K. F., and Peterson, L. D., "Limitations of State-Space System Identification Algorithms for Structures with High Modal Density," *Proceedings of the 12th International Modal Analysis Conference*, Honolulu, HI, Jan. 1994, pp. 633–640.

²²Peterson, L. D. "Efficient Computation of the Eigensystem Realization Algorithm," *Journal of Guidance, Control and Dynamics*, Vol. 18, No. 3, 1995, pp 395–403.

²³Golub, G. H. and Van Loan, C. F., *Matrix Computations*, Johns Hopkins University Press, 1983.

²⁴Blevins, R. D., *Formulas for Natural Frequency and Mode Shape*, Krieger Publishing, Malabar, FL, 1993.

²⁵Yang, T. Y., *Finite Element Structural Analysis*, Prentice-Hall, Englewood Cliffs, NJ, 1986.

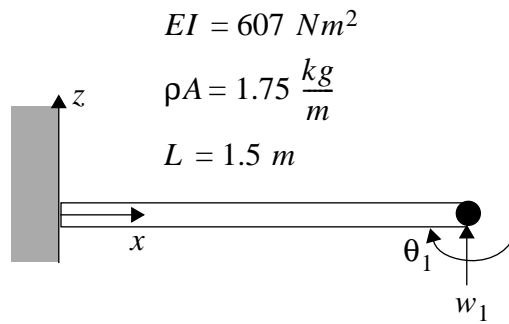


Figure 1: Two-DOF Cantilevered Beam Model

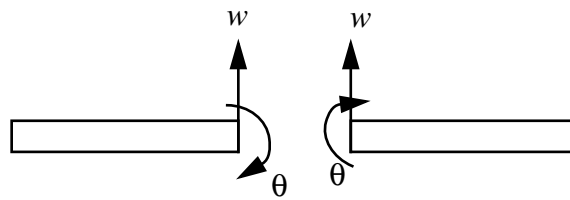


Figure 2: Two Free-Free Beam Components for CMS Example



Figure 3: Cantilevered Beam Test Setup

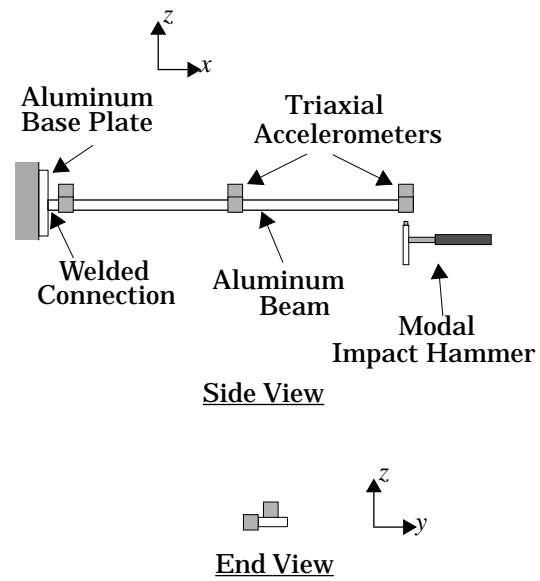


Figure 4: Schematic of Cantilevered Beam Test Structure

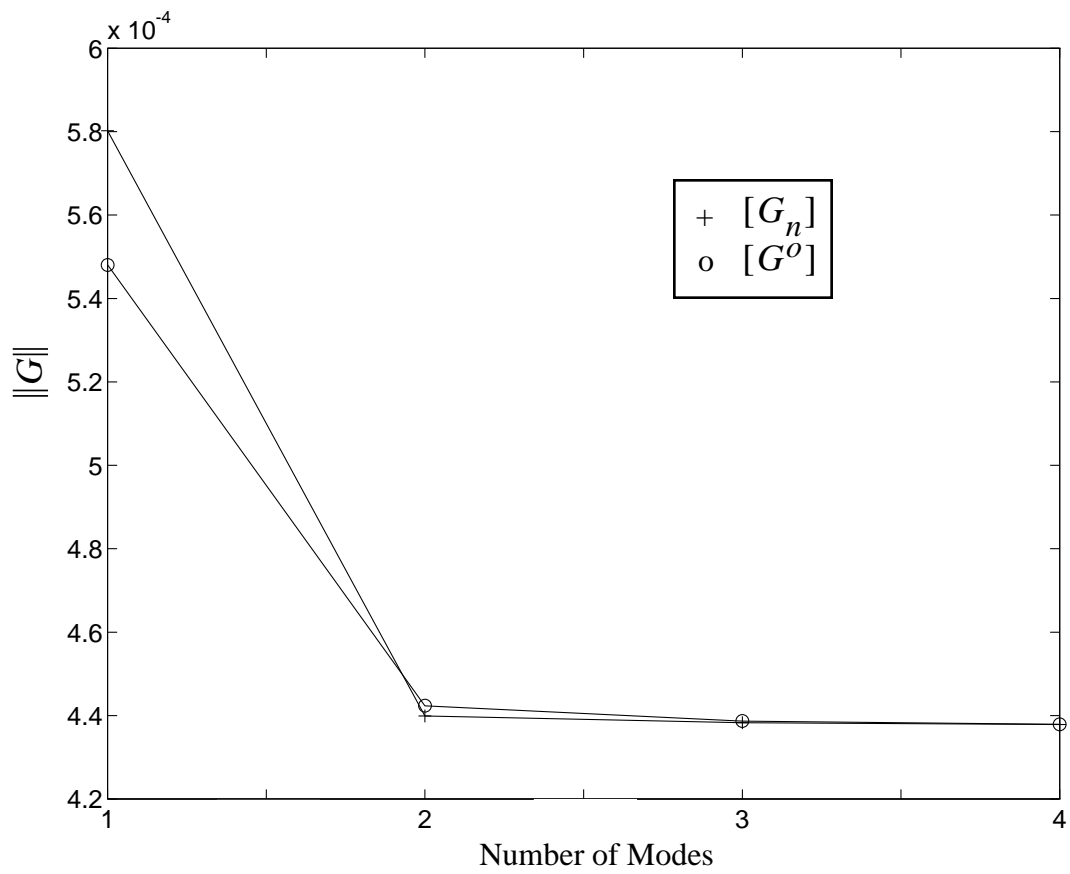


Figure 5: Flexibility Convergence Plot for Cantilevered Beam

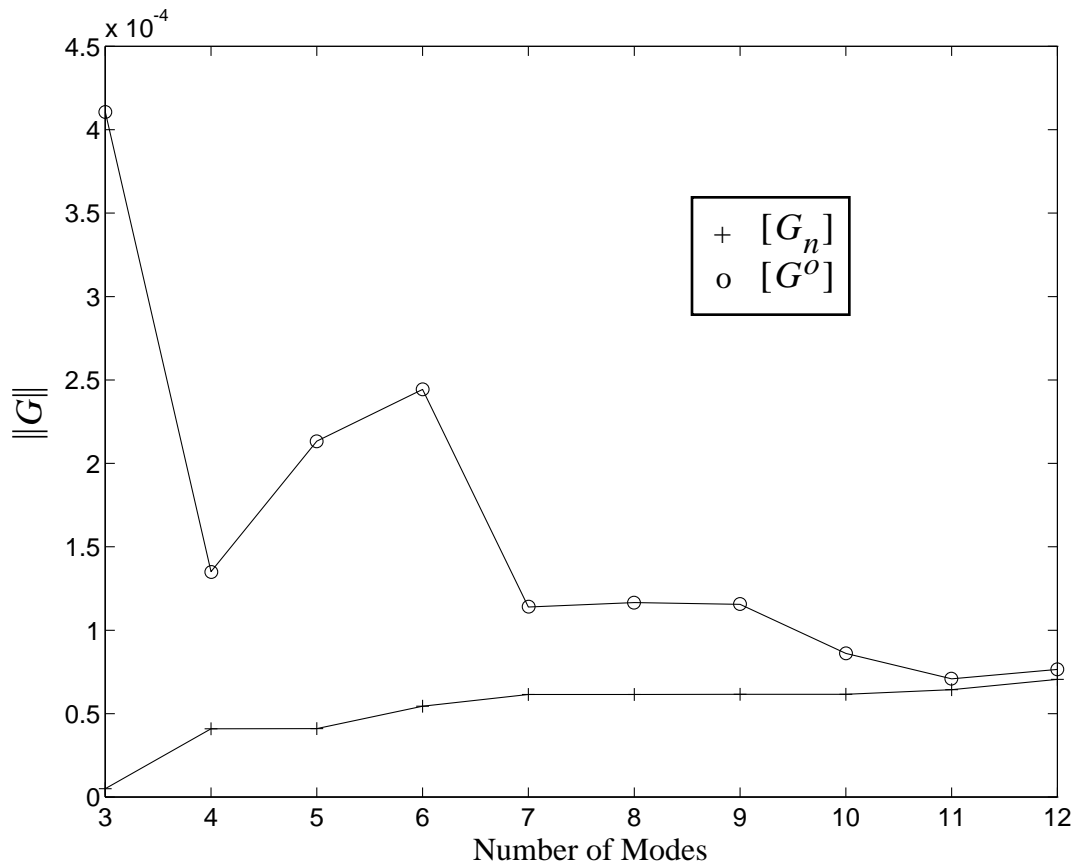


Figure 6: Flexibility Convergence Plot for Planar Engine Cradle Structure

List of Figure Captions

Figure 1: 2-DOF Cantilevered Beam Model

Figure 2: Two Free-Free Beam Components for CMS Example

Figure 3: Cantilevered Beam Test Setup

Figure 4: Schematic of Cantilevered Beam Test Structure

Figure 5: Flexibility Convergence Plot for Cantilevered Beam

Figure 6: Flexibility Convergence Plot for Planar Engine Cradle Structure